Monte Carlo simulation of the tight-binding model of graphene with partially screened Coulomb interactions

Dominik Smith[1] and Lorenz von Smekal[1,2]

[1]*Theoriezentrum, Institut für Kernphysik, TU Darmstadt, 64289 Darmstadt, Germany*
[2]*Institut für Theoretische Physik, Justus-Liebig-Universität, 35392 Giessen, Germany*

We report on hybrid Monte Carlo simulations of the tight-binding model with long-range Coulomb interactions for the electronic properties of graphene. We investigate the spontaneous breaking of sublattice symmetry corresponding to a transition from the semimetal to an antiferromagnetic insulating phase. Our short-range interactions thereby include the partial screening due to electrons in higher energy states from *ab initio* calculations based on the constrained random phase approximation [T. O. Wehling *et al.*, Phys. Rev. Lett. **106**, 236805 (2011)]. In contrast to a similar previous Monte Carlo study [M. V. Ulybyshev *et al.*, Phys. Rev. Lett. **111**, 056801 (2013)], we also include a phenomenological model that describes the transition to the unscreened bare Coulomb interactions of graphene at half-filling in the long-wavelength limit. Our results show, however, that the critical coupling for the antiferromagnetic Mott transition is largely insensitive to the strength of these long-range Coulomb tails. They hence confirm the prediction that suspended graphene remains in the semimetal phase when a realistic static screening of the Coulomb interactions is included.

I. INTRODUCTION

In recent years, much interest has arisen in the study of graphene, an allotrope of carbon which consists of a single layer of atoms, arranged on a hexagonal ("honeycomb") lattice. It has become increasingly clear that such a system, despite (or rather due to) its very simple structure, possesses a large variety of unusual properties. These range from extreme mechanical strength and lightness, over unique electronic properties to a number of anomalous quantum effects, which make graphene a very attractive candidate for a wide range of technological applications (for extensive reviews of the properties of graphene, see Refs. [1–4]). Moreover, from a theoretical perspective it has become clear that graphene can serve as a model system for a large number of concepts from high-energy physics, ranging from topological phase transitions, chiral symmetry breaking and supersymmetry to quantum gravity (for more on the connections between graphene and high-energy physics see, e.g., Refs. [5–12] and references therein).

This has motivated the application of well-established field-theory methods from particle physics as effective descriptions of the low-energy electronic excitations in graphene. Since the relevant coupling constant for the Coulomb interactions can thereby be as large as $\alpha_{\text{eff}} = e^2/(\hbar v_F)$ in suspended graphene, where $v_F \approx c/300$ is the Fermi velocity, one needs to describe a strongly coupled fermionic system with an effective coupling $\alpha_{\text{eff}} \approx 300/137 \approx 2.2$. This suggests the application of non-perturbative methods. In particular, graphene at half-filling can be efficiently simulated via hybrid Monte Carlo method, a widely used algorithm in lattice gauge theory, both in the low-energy (long-wavelength) limit [13–22] where graphene is well-described by a variant of quantum electrodynamics in $2 + 1$ dimensions and as a full theory, which is valid on length scales down to the interatomic distance $a \approx 1.42$ Å [23–27].

An open question that is of immediate consequence to technological applications is whether graphene, which is known to be an electric conductor when affixed to a number of different substrates, can develop a band gap under proper circumstances. This could correspond to a spontaneous breaking of the symmetry under exchange of the two triangular sublattices with strong analogies to chiral symmetry breaking in relativistic field theory. A substrate generates dielectric screening which lowers the effective fine-structure constant α_{eff} of the system. The expectation is that if screening is reduced, when α_{eff} becomes larger than some critical coupling α_c, a phase transition to a gapped phase occurs. In order to be physically realizable, α_c should be smaller than $\alpha_{\text{eff},0} \approx 300/137 \approx 2.2$, which is the upper bound in suspended graphene, where screening is minimal.

Experiments have provided evidence that graphene in vacuum is in fact a conductor [28,29], while analytical calculations [30–34] and simulations [13–15,18,19,25], which assumed that the electromagnetic interactions of π-band electrons (the relevant degrees of freedom for the electronic properties) are essentially unmodified Coulomb interactions, supported the scenario of a gapped phase for $\alpha_{\text{eff}} > \alpha_c \approx 1$, well within the accessible region. The origin of this disparity must thus be investigated.

Recently, it was suggested that additional screening (independent of the reduction of α_{eff} by the substrate) of the two-body Coulomb interactions, by electrons in the lower σ bands and other higher energy states of the carbon sheet itself [35], provides a mechanism that moves α_c to larger values, outside of the physical region.[1] In Ref. [26], hybrid Monte Carlo simulations of the tight-binding model with an instantaneous two-body potential generated by a Hubbard field were carried out (based on the framework developed in Refs. [23,24]), which addressed the issue of σ-band screening. For these simulations, a screened Coulomb potential was chosen which used the results of a calculation within the

---

[1]Another mechanism which has been proposed is a reshaping of the Dirac cone due to renormalization of the Fermi velocity [28,36,37]. The magnitude of this effect is likely much smaller than that of screening and, in any case, the inclusion of this effect is automatic in lattice simulations.

constrained random phase approximation (cRPA) [35] for on-site repulsion, the nearest-neighbor, next-to-nearest-neighbor, and third-nearest-neighbor interactions at short distances. At longer distances, it was assumed that the potential falls off as $\sim 1/(\epsilon_\sigma r)$, where the constant $\epsilon_\sigma \approx 1.41$ was adjusted to match the third-nearest-neighbor term. It was shown that for this particular choice of potential, the critical coupling for the antiferromagnetic Mott transition is moved to $\alpha_c \approx 3.14$, which is outside of the physically accessible region and thus agrees with the experimental observation.

In this work, we conduct simulations similar to those of Ref. [26], however, with a more realistic description of the partial screening of the Coulomb interactions at larger distances: instead of assuming the constant reduction in the strength of the long-range Coulomb tails, by ϵ_σ, which quite naturally necessitates an increased effective coupling to compensate that, we use the phenomenological model also given in Ref. [35] to construct a partially screened Coulomb interaction with a momentum dependent $\epsilon_\sigma(\vec{k})$, which smoothly turns into the unscreened Coulomb potential corresponding to $\epsilon_\sigma \to 1$ in the long-wavelength limit. This reflects the fact that the high-energy states in graphene do not screen the long-range Coulomb tails in the interactions of the π-band electrons as demonstrated explicitly in Ref. [35]. Because the density of states in the π bands furthermore vanishes at the Dirac points in the band structure of graphene, so does the static Lindhard susceptibility in the long-wavelength limit. There is thus no screening of the long-range Coulomb tails from the π bands in graphene at half-filling in the semimetal phase either. The presence of unscreened long-range Coulomb interactions is one of the distinctive features of the interactions in graphene.

The effects of on-site repulsion versus nearest and few next-to-nearest-neighbor interactions have been studied in Hubbard models at length. Depending on their relative strengths a variety of competing phases has been predicted such as spin and charge-density-wave phases [38–40], spin liquids [41,42], or topological insulators [43]. In order to address the long-standing question whether the long-range Coulomb interactions in graphene favor any of these insulating phases, we therefore decided to rather leave those Coulomb tails unmodified. The fact that our results basically agree with those of Ref. [26] indicates that they have little effect on the antiferromagnetic spin-density-wave formation investigated here.

This paper is structured as follows. In the next section we present a detailed review of the theoretical framework for the hybrid Monte Carlo simulation of the hexagonal graphene lattice which is employed in this work, including a discussion of the partially screened Coulomb potential which is used. We then present the results of the investigation of the semimetal-insulator phase transition, including a more detailed comparison with the results of Ref. [26], which we have reproduced for cross-checking purposes. In the last section, we discuss our results and provide an outlook on future projects.

A few comments on the units and conventions used throughout this paper. We use the natural system of units of high-energy physics, i.e., $c \equiv 1$ and $\hbar \equiv 1$. Furthermore, we use the Gaussian system of electromagnetic units, in which the Coulomb potential is simply $1/r$. These conventions imply the relation $\alpha = e^2 \approx 1/137$ between the elementary charge and the (dimensionless) fine-structure constant. We then have the

freedom to express all physical quantities using either a basic unit of energy or of length. We generally use electron-volt (eV) as the fundamental unit (the potential then has a dimension of energy). However, in some cases (where experimental results are concerned), a value in meters will be also given for lengths. The two are related via 10^{-7} m ≈ 0.506 eV^{-1}. When conducting Fourier analysis, we write normalization factors of $1/(2\pi)$ only in front of momentum-space integrals, as is customary in high-energy physics.

II. THE SETUP

In this section, the central components of the lattice simulation of the interacting tight-binding theory of graphene are derived. We aim to give a rather comprehensive review, which should hopefully be useful for readers from various backgrounds. We therefore provide many technical details, and where we refer to existing literature we fill in various steps that where omitted in the original articles.

The section is structured as follows. We begin with a general discussion of the graphene lattice and of the way we treat boundary conditions, followed by the derivation of the path-integral formulation of the grand-canonical partition function Z of the interacting tight-binding theory. This forms the basis of everything that follows. The derivation of Z was first worked out in Refs. [23,24]. We review the essential steps and provide an explicit representation of the fermion matrix. Based on this formulation, in the following paragraph a detailed discussion of the hybrid Monte Carlo algorithm is then presented, which we use to generate lattice configurations. This includes a step-by-step derivation of the molecular-dynamics force terms, which have not been given explicitly in the literature before. Next, we present the derivation of an expression for the order parameter for sublattice symmetry breaking in terms of elements of the inverse fermion matrix, which is used for measurements. We then discuss the second-order fermion operator first derived in Ref. [26], specifically showing which aspects of the preceding derivations are changed. And finally, we discuss in detail how we obtain an expression for the partially screened Coulomb potential using the cRPA results and the phenomenological dielectric screening function presented in Ref. [35].

A. The graphene lattice

Consider a two-dimensional triangular lattice, spanned by the basis vectors

$$\vec{e}_1 = (\sqrt{3}, 0)\, a, \quad \vec{e}_2 = \left(\frac{\sqrt{3}}{2}, \frac{3}{2} \right) a, \tag{1}$$

such that each lattice point can be reached by $\vec{r} = m\vec{e}_1 + n\vec{e}_2$ for some integers m, n. Here, we have introduced $a = 1.42$ Å ($\approx 0.71 \times 10^{-3}$ eV^{-1}). The hexagonal graphene lattice can be constructed from these vectors by assigning a two-component basis to each lattice point, such that one carbon atom sits exactly on each point and another one is reached by a translation

$$\vec{\delta} = (0, 1)\, a. \tag{2}$$

It is obvious from this construction that a is the interatomic spacing. The above is equivalent to the statement that graphene is composed of two inequivalent triangular sublattices, which

sit a translation along $\vec{\delta}$ apart. We will refer to these as sublattices A and B.

By restricting (m,n) to $m \in [0, L_m - 1]$, $n \in [0, L_n - 1]$, one obtains a graphene sheet shaped like a parallelogram. In the following, we always assume that L_m, L_n are both even. It is our goal to simulate rectangular graphene sheets with periodic boundary conditions. We thus impose

$$(m + L_m, n) \equiv (m,n), \quad (m, n + L_n) \equiv (m - L_n/2, n). \quad (3)$$

The periodic boundary conditions, invariant under discrete hexagonal lattice translations, are a technical device to reduce boundary effects. As such they are frequently used in lattice simulations when one is (as we are here) interested in bulk thermodynamics. Their main purpose is not so much to mimic physical boundary conditions in experiments but to provide a reasonably rapid approach towards the infinite volume limit with growing system size.

To construct a finer rectangular system of coordinates whose basis vectors align with the axes of periodicity, and in which points on both sublattices can be uniquely identified, consider the new set of basis vectors given by

$$\vec{e}_1{}' = \vec{e}_1/2 = (\sqrt{3}/2, 0)\,a, \quad \vec{e}_2{}' = \vec{\delta}/2 = (1/2, 0)\,a. \quad (4)$$

The majority of points on the finer grid defined by these vectors are empty, but every point on the hexagonal lattice can be written as $\vec{r}\,' = x\vec{e}_1{}' + y\vec{e}_2{}'$ with

$$x = 2m + n, \quad y = 3n + 2P_{AB}, \quad (5)$$

where $P_{AB} = 0$ on sublattice A and $P_{AB} = 1$ on sublattice B. Periodicity is expressed in this system by restricting x, y to $x \in [0, 2L_m - 1]$, $y \in [0, 3L_n - 1]$ and identifying

$$(x + 2L_m, y) \equiv (x, y), \quad (x, y + 3L_n) \equiv (x, y). \quad (6)$$

The rectangular coordinate system $\vec{e}_1{}'$, $\vec{e}_2{}'$ will be convenient for Fourier analysis.

Figure 1 shows an example in which $L_m = 6$, $L_n = 4$. The axes of both coordinate systems are shown, including an indexing scheme (discussed below). The periodic system can be constructed by repeating the figure. The figure is drawn such that this is well-defined: every lattice point on the boundary exists exactly once.
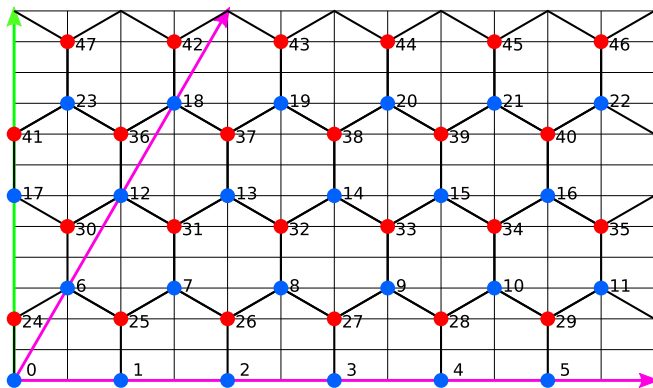

FIG. 1. (Color online) Indexing scheme and coordinate systems for $L_m = 6$, $L_n = 4$, $N_t = 1$. Blue dots are A sites and red dots are B sites.

In the following section, a Euclidean (imaginary) time dimension will be introduced. One can thus imagine additional lattices associated with integer values of an additional coordinate τ. We store fields (functions defined over the hexagonal lattice) as one-dimensional arrays. We thus require a scheme to uniquely assign an index to each lattice site. Consider a graphene lattice of spatial dimensions L_m and L_n with N_t time slices. There are thus altogether $2 \times L_m \times L_n \times N_t$ sites (the factor 2 is due to the two sublattices). We introduce lexicographically ordered site indices in such a way that the entire A sublattice is counted first, and the B sublattice is counted second. The index for a site (m, n, τ) in one sublattice is thus calculated as

$$\text{index} = m + n\,L_m + \tau\,(L_m L_n) + P_{AB}\,(L_m L_n N_t). \quad (7)$$

The example in Fig. 1 corresponds to $N_t = 1$.

B. Path integral formulation of the partition function

We wish to express the grand-canonical partition function $Z = \mathrm{Tr}\,e^{-\beta H}$ of the tight-binding model as a functional integral. This is essential for a Monte Carlo simulation, since in doing so one replaces operators by field variables, which can be stored in a computer. Here, $\beta = 1/k_B T$ (which we will express in units of eV^{-1}) refers to the temperature of the electron gas, which does not include lattice vibrations and thus should not be confused with the temperature of the graphene sheet (T can be arbitrarily large here, whereas physical graphene would be destroyed above some temperature). We use the coherent state functional integral formalism (see, e.g., Ref. [44] for an introduction) to obtain Z. This formalism derives from the fact that the Fock space of a fermionic many-body system is spanned by a complete basis of fermionic coherent states.

The starting point is the Hamiltonian of the interacting tight-binding model,

$$
\begin{aligned}
H = {} & H_{\text{tb}} + H_c + H_m \\
= {} & -\kappa \sum_{\langle x, y \rangle, s} (a^\dagger_{x,s} a_{y,s} + a^\dagger_{y,s} a_{x,s}) + \frac{1}{2} \sum_{x,y} q_x V_{xy} q_y \\
& + \sum_x m_s (a^\dagger_{x,+1} a_{x,+1} + a_{x,-1} a^\dagger_{x,-1}),
\end{aligned}
\quad (8)
$$

where $a^\dagger_{x,s}, a_{x,s}$ are creation and annihilation operators for electronic excitations in the π-bands with the usual fermionic anti-commutation relations,

$$\{a^\dagger_i, a^\dagger_j\} = \{a_i, a_j\} = 0, \quad \{a^\dagger_i, a_j\} = \delta_{ij}. \quad (9)$$

The first sum in Eq. (8) runs over all pairs of nearest neighbors (including those pairs where a periodic boundary is crossed) and defines the free tight-binding Hamiltonian H_{tb}. The second and the third sums run over all pairs of sites in the interaction Hamiltonian H_c, and all sites in the "mass term" H_m, respectively. The electron spin is labeled by $s = \pm 1$. The constant κ is the hopping parameter, which is fixed by experiment to $\kappa \approx 2.8$ eV. The mass term is "staggered" with respect to the two independent sublattices, which means that

$$
m_s = \begin{cases} +m, & x \in A, \\ -m, & x \in B. \end{cases}
\quad (10)
$$

This term is added to explicitly break sublattice symmetry. This is required for technical reasons. In particular, it removes zero modes from the fermion operator, such that the fermion matrix can be inverted. Physical results are obtained by extrapolating to $m \to 0$. Moreover note that the staggering in H_m has the opposite sign for each spin component $s = \pm 1$, and m_s thus acts as an external field for spin-density-wave formation.

We have furthermore introduced the charge operator

$$q_x = a^\dagger_{x,1} a_{x,1} + a^\dagger_{x,-1} a_{x,-1} - 1 = a^\dagger_{x,1} a_{x,1} - a_{x,-1} a^\dagger_{x,-1}, \tag{11}$$

where the constant is added to make the system neutral at half-filling.

V_{xy} are the elements of a matrix describing instantaneous two-body interactions. It need not be further specified at this point, other than that it be positive-definite and have the dimension of energy (or inverse length). We use a partially screened Coulomb potential in this work, which is discussed in detail in Sec. II F below.

To proceed, we apply a few transformations to explicitly see how the antiferromagnetic Mott transition at half-filling can be simulated without a fermion sign problem [38].[2] The reason for this will become clear once we have obtained the explicit form of the fermion operator. In particular, a mass term without the spin staggering, as an external field for charge-density-wave formation, will be seen to introduce such a sign problem. First, we introduce "hole" creation and annihilation operators $b^\dagger_x, b_x$ for the electrons with $s = -1$ and from now on use the notation

$$a_x = a_{x,1}, a^\dagger_x = a^\dagger_{x,1}, b^\dagger_x = a_{x,-1}, b_x = a^\dagger_{x,-1}. \tag{12}$$

The charge operator is then expressed as

$$q_x = a^\dagger_x a_x - b^\dagger_x b_x, \tag{13}$$

and the Hamiltonian becomes

$$H = \sum_{\langle x,y \rangle} (-\kappa)(a^\dagger_x a_y - b^\dagger_x b_y + \text{h.c.}) + \sum_{x,y} q_x V_{xy} q_y$$
$$+ \sum_x m_s (a^\dagger_x a_x + b^\dagger_x b_x). \tag{14}$$

Next, we redefine the $b^\dagger_x, b_x$ by flipping the sign on one of the sublattices, say B:

$$b_x, b^\dagger_x \longrightarrow -b_x, -b^\dagger_x \quad \forall\, x \in B. \tag{15}$$

This is an allowed transformation since it preserves the anticommutation relations. It induces a sign-flip in the nearest-neighbor term:

$$H_{\text{tb}} = \sum_{\langle x,y \rangle} (-\kappa)(a^\dagger_x a_y - b^\dagger_x b_y + \text{H.c.})$$
$$\longrightarrow \sum_{\langle x,y \rangle} (-\kappa)(a^\dagger_x a_y + b^\dagger_x b_y + \text{H.c.}). \tag{16}$$

---

[2]This refers to an indefinite sign or a complex measure introduced by the fermions which can make Monte-Carlo simulations impossible or at least extremely difficult.

We now introduce the fermionic coherent states. These states are constructed using anticommuting Grassmann variables in the following way. Consider a set of creation and annihilation operators $(a_\alpha, a^\dagger_\alpha)$, where the index α labels all single-particle states of the system. Now associate with them a set of Grassmann numbers $(\xi_\alpha, \xi^*_\alpha)$ such that for each a_α there is a ξ_α and for each $a^\dagger_\alpha$ there is a ξ^*_α. The coherent states are then

$$|\xi\rangle = e^{-\sum_\alpha \xi_\alpha a^\dagger_\alpha} |0\rangle, \quad \langle \xi| = \langle 0| e^{-\sum_\alpha a_\alpha \xi^*_\alpha}. \tag{17}$$

The $|\xi\rangle$ are right eigenstates of the annihilation operators, while the $\langle \xi|$ are left eigenstates of the creation operators. The completeness relation on the Fock space is given in terms of these states as

$$\int \left(\prod_\alpha d\xi^*_\alpha\, d\xi_\alpha \right) e^{-\sum_\alpha \xi^*_\alpha \xi_\alpha} |\xi\rangle \langle \xi| = \mathbf{1}, \tag{18}$$

where the product and sum run over all single-particle states. Moreover, the trace of a bosonic operator A can be expressed as

$$\text{Tr}\, A = \int \left(\prod_\alpha d\xi^*_\alpha\, d\xi_\alpha \right) e^{-\sum_\alpha \xi^*_\alpha \xi_\alpha} \langle -\xi| A |\xi\rangle. \tag{19}$$

We can now construct coherent states for the Fock space of fermionic quasiparticles and holes, generated by the operators $a_x, a^\dagger_x, b_x, b^\dagger_x$ as

$$\langle \psi, \eta| = \langle 0| e^{-\sum_x (a_x \psi^*_x + b_x \eta^*_x)}, \quad |\psi, \eta\rangle = e^{-\sum_x (\psi_x a^\dagger_x + \eta_x b^\dagger_x)} |0\rangle. \tag{20}$$

Note that they are exactly of the form given in Eq. (17), if one understands the index α to label spin and position states. Introducing two different symbols ψ, η is entirely a matter of notational convenience. Using these states, we can now express the grand-canonical partition function as

$$Z = \text{Tr}\, e^{-\beta H} = \int \left(\prod_x d\psi^*_x\, d\psi_x\, d\eta^*_x\, d\eta_x \right)$$
$$\times e^{-\sum_x (\psi^*_x \psi_x + \eta^*_x \eta_x)} \langle -\psi, -\eta| e^{-\beta H} |\psi, \eta\rangle. \tag{21}$$

In order to deal with the product $\langle -\psi, -\eta| e^{-\beta H} |\psi, \eta\rangle$, which appears in the integral consider the following. If $F(a^\dagger_\alpha, a_\alpha)$ is a *normal ordered* function of creation and annihilation operators, then its matrix element between coherent states is given by

$$\langle \xi| F(a^\dagger_\alpha, a_\alpha)|\xi'\rangle = F(\xi^*_\alpha, \xi'_\alpha) e^{\sum_\alpha \xi^*_\alpha \xi'_\alpha}. \tag{22}$$

Using our notation which distinguishes position and spin states this becomes

$$\langle \psi, \eta| F(a^\dagger_x, a_x, b^\dagger_x, b_x)|\psi', \eta'\rangle$$
$$= F(\psi^*_x, \psi'_x, \eta^*_x, \eta'_x) e^{\sum_x \psi^*_x \psi'_x + \eta^*_x \eta'_x}. \tag{23}$$

If $e^{-\beta H}$ was a normal ordered function, we would be done, for then we could use Eq. (23) and obtain an expression for Z in which no operators appear. This is, however, not generally true, even if H is normal ordered. We proceed by splitting the exponential into N_t separate factors,

$$e^{-\beta H} = e^{-\delta H} e^{-\delta H} \dots e^{-\delta H} \quad (\delta = \beta/N_t), \tag{24}$$

and inserting a complete set of coherent states via the unity in Eq. (18) between subsequent ones. Using an index t to label

the coherent states associated with each time slice,

$$\langle \psi_t, \eta_t | = \langle 0 | e^{-\sum_x (a_x \psi_{x,t}^* + b_x \eta_{x,t}^*)},$$
$$|\psi_t, \eta_t \rangle = e^{-\sum_x (\psi_{x,t} a_x^\dagger + \eta_{x,t} b_x^\dagger)} |0\rangle, \tag{25}$$

we obtain the expression

$$\mathrm{Tr}\, e^{-\beta H} = \int \prod_{t=0}^{N_t-1} \left(\prod_x d\psi_{x,t}^* \, d\psi_{x,t} \, d\eta_{x,t}^* \, d\eta_{x,t} \right)$$
$$\times e^{-\sum_x (\psi_{x,t+1}^* \psi_{x,t+1} + \eta_{x,t+1}^* \eta_{x,t+1})}$$
$$\times \langle \psi_{t+1}, \eta_{t+1} | e^{-\delta H} | \psi_t, \eta_t \rangle. \tag{26}$$

From Eq. (26) it is clear that t can be understood as labeling the Euclidean time direction. Antiperiodic boundary conditions

$$\psi_{x,N_t} = -\psi_{x,0}, \quad \eta_{x,N_t} = -\eta_{x,0} \tag{27}$$

have been introduced here to make this compact notation possible. They are simply the result of the minus sign in Eq. (19), or inside the $\langle -\psi, -\eta |$ states in Eq. (21), and reflect the fermionic statistics of the electronic quasiparticles.

The matrix elements in Eq. (26) are then treated in the following way. Assuming that the Hamilton operator is expressed in normal ordered form, the leading terms in an expansion of $e^{-\delta H}$, which are not normal ordered are $\mathcal{O}(\delta^2)$. Discarding these terms, i.e., treating $e^{-\delta H}$ as if it was normal ordered, therefore implies a discretization error $\mathcal{O}(\delta)$, which vanishes with $N_t \to \infty$. Hence δ can be visualized as the lattice spacing of the discretization in the Euclidean time direction.

We require a normal ordered form of H to proceed. In this, the only term requiring special attention is the diagonal term of H_c, since this is the only term which generates something other than a trivial change of sign when brought into normal order. Applying normal ordering to this term yields

$$q_x V_{xx} q_x = -2V_{xx}\, a_x^\dagger a_x\, b_x^\dagger b_x + V_{xx}(a_x^\dagger a_x + b_x^\dagger b_x)$$
$$= :q_x V_{xx} q_x: + V_{xx}(a_x^\dagger a_x + b_x^\dagger b_x). \tag{28}$$

With $n_{x,\uparrow} = a_x^\dagger a_x$ and $n_{x,\downarrow} = 1 - b_x^\dagger b_x$ one thus identifies the usual Hubbard model on-site repulsion $U = V_{xx}$.

Using Eq. (23), we now evaluate the matrix elements in Eq. (26) and obtain

$$\mathrm{Tr}\, e^{-\beta H} = \int \prod_{t=0}^{N_t-1} \left(\prod_x d\psi_{x,t}^* \, d\psi_{x,t} \, d\eta_{x,t}^* \, d\eta_{x,t} \right) \exp\left\{ -\delta \left[\frac{1}{2} \sum_{x,y} Q_{x,t+1,t} V_{xy} Q_{y,t+1,t} \right.\right.$$
$$- \sum_{\langle x,y \rangle} \kappa (\psi_{x,t+1}^* \psi_{y,t} + \psi_{y,t+1}^* \psi_{x,t} + \eta_{y,t+1}^* \eta_{x,t} + \eta_{x,t+1}^* \eta_{y,t})$$
$$+ \sum_x m_s (\psi_{x,t+1}^* \psi_{x,t} + \eta_{x,t+1}^* \eta_{x,t}) + \frac{1}{2} \sum_x V_{xx}(\psi_{x,t+1}^* \psi_{x,t} + \eta_{x,t+1}^* \eta_{x,t}) \bigg]$$
$$- \sum_x [\psi_{x,t+1}^*(\psi_{x,t+1} - \psi_{x,t}) + \eta_{x,t+1}^*(\eta_{x,t+1} - \eta_{x,t})] \bigg\}. \tag{29}$$

Here we have introduced the "charge field"

$$Q_{x,t,t'} = \psi_{x,t}^* \psi_{x,t'} - \eta_{x,t}^* \eta_{x,t'}. \tag{30}$$

To simulate Eq. (29) via standard Monte Carlo methods, one wishes to eliminate the Grassmann variables and ultimately deal only with regular complex numbers. The customary way to achieve this, which is applied to various systems with fermionic degrees of freedom, is to integrate out the fermion fields and to rewrite the fermionic part of the action as a determinant, which then can be sampled stochastically using pseudofermion sources. To this end, a Gaussian integral of the form

$$\int \left(\prod_{m=1}^n d\chi_m^* \, d\chi_m \right) e^{-\sum_{i,j=1}^n \chi_i^* H_{ij} \chi_j} \propto (\det H)^{\pm 1}, \tag{31}$$

must be carried out (this identity holds for both complex commuting variables χ_i with the negative sign on the right-hand side, in case of which H must have a positive Hermitian part, and for Grassmann variables with the positive sign and no restrictions on H). This is impossible for the current form of Eq. (29) since forth powers of the Grassmann ("field") variables appear. We can eliminate these at the expense of introducing a scalar auxiliary field ϕ by applying the Hubbard-Stratonovich transformation,

$$\exp\left(-\frac{\delta}{2} \sum_{t=0}^{N_t-1} \sum_{x,y} Q_{x,t+1,t} V_{xy} Q_{y,t+1,t} \right) \propto \int \mathcal{D}\phi \, \exp\left(-\frac{\delta}{2} \sum_{t=0}^{N_t-1} \sum_{x,y} \phi_{x,t} V_{xy}^{-1} \phi_{y,t} - i\,\delta \sum_{t=0}^{N_t-1} \sum_x \phi_{x,t} Q_{x,t+1,t} \right). \tag{32}$$

We will refer to ϕ as the Hubbard-Coulomb field. It has the dimension of energy or inverse length as usual. A constant factor in Eq. (32) is omitted, since it can be absorbed into the measure. Here we have introduced the shorthand notation

$$\mathcal{D}\phi = \left(\prod_{t=0}^{N_t-1} \prod_x d\phi_{x,t} \right), \tag{33}$$

which we will use for the remainder of the paper for any generic field χ. Applying the transformation, we obtain

$$
\mathrm{Tr}\, e^{-\beta H} = \int \mathcal{D}\psi\, \mathcal{D}\psi^*\, \mathcal{D}\eta\, \mathcal{D}\eta^*\, \mathcal{D}\phi\, \exp\left\{-\delta \sum_{t=0}^{N_t-1}\left[\frac{1}{2}\sum_{x,y}\phi_{x,t}V_{xy}^{-1}\phi_{y,t} + \sum_x i\phi_{x,t}Q_{x,t+1,t}\right.\right.
$$

$$
- \sum_{\langle x,y\rangle}\kappa(\psi_{x,t+1}^*\psi_{y,t} + \psi_{y,t+1}^*\psi_{x,t} + \eta_{y,t+1}^*\eta_{x,t} + \eta_{x,t+1}^*\eta_{y,t})
$$

$$
+ \sum_x m_s(\psi_{x,t+1}^*\psi_{x,t} + \eta_{x,t+1}^*\eta_{x,t}) + \frac{1}{2}\sum_x V_{xx}(\psi_{x,t+1}^*\psi_{x,t} + \eta_{x,t+1}^*\eta_{x,t})\Bigg]
$$

$$
\left.\left.- \sum_{t=0}^{N_t-1}\sum_x[\psi_{x,t+1}^*(\psi_{x,t+1} - \psi_{x,t}) + \eta_{x,t+1}^*(\eta_{x,t+1} - \eta_{x,t})]\right\}. \right. \tag{34}
$$

This expression contains no fourth powers. By introducing a matrix M, which is defined in terms of its elements as

$$
M_{(x,t)(y,t')} = \delta_{xy}(\delta_{tt'} - \delta_{t-1,t'}) - \kappa\frac{\beta}{N_t}\sum_{\vec{n}}\delta_{y,x+\vec{n}}\delta_{t-1,t'} + m_s\frac{\beta}{N_t}\delta_{xy}\delta_{t-1,t'} + \frac{V_{xx}}{2}\frac{\beta}{N_t}\delta_{xy}\delta_{t-1,t'} + i\phi_{x,t}\frac{\beta}{N_t}\delta_{xy}\delta_{t-1,t'}. \tag{35}
$$

We can rewrite Eq. (34) as

$$
\mathrm{Tr}\, e^{-\beta H} = \int \mathcal{D}\psi\, \mathcal{D}\psi^*\, \mathcal{D}\eta\, \mathcal{D}\eta^*\, \mathcal{D}\phi\, \exp\left[-\frac{\delta}{2}\sum_{t=0}^{N_t-1}\sum_{x,y}\phi_{x,t}V_{xy}^{-1}\phi_{y,t} - \sum_{t,t'=0}^{N_t-1}\sum_{x,x'}\left(\psi_{x,t}^* M_{(x,t)(x',t')}\psi_{x',t'} + \eta_{x,t}^* M_{(x,t)(x',t')}^*\eta_{x',t'}\right)\right]. \tag{36}
$$

Here, M^* means complex conjugate (of individual elements), not the Hermitian conjugate (which we will write as $M^\dagger$). The notation (x,t) here is understood to imply that the indices labeling matrix elements of M enumerate pairs of coordinates x and t.

We can now carry out the Gaussian integration and obtain

$$
\mathrm{Tr}\, e^{-\beta H} = \int \mathcal{D}\phi\, \det M^*(\phi)\det M(\phi)\exp\left(-\frac{\delta}{2}\sum_{t=0}^{N_t-1}\sum_{x,y}\phi_{x,t}V_{xy}^{-1}\phi_{y,t}\right)
$$

$$
= \int \mathcal{D}\phi\, \det\left[M(\phi)M^\dagger(\phi)\right]\exp\left(-\frac{\delta}{2}\sum_{t=0}^{N_t-1}\sum_{x,y}\phi_{x,t}V_{xy}^{-1}\phi_{y,t}\right). \tag{37}
$$

Here, we can see explicitly why it was convenient to introduce hole operators for the spin-down states. In absence of magnetic fields and spin dependent interactions, the true spin of the electrons formally plays the role of a flavor quantum number. The corresponding flavor symmetry entails that, without mass term, both spin degrees of freedom lead to the same fermion matrix. By introducing hole operators for one species, we basically changed the sign of the charge of the corresponding quasiparticles and hence obtain a manifestly real and positive contribution $\det(MM^\dagger)$ in the measure for the product of both flavors. Note, however, that because $\det M^*(m_s) = \det M(-m_s)$, it is only the mass term, which can lead to truly complex fermion determinants. Without it, M would have definite hHermiticity properties for each spin. The decisive assumption for a real product of fermion matrices here is the spin staggering of the mass term. Without introduction of hole operators for one of the spin states, both fermionic quasiparticles would have the same charge, and hence the same sign in the last term of Eq. (35), but the opposite sign in the mass term proportional to m_s. Only if that were not the case, would the product of fermion determinats not be real.

Equation (37) is now in a form suitable for simulation via hybrid Monte Carlo. Note that the only remaining integration is over the Hubbard-Coulomb field ϕ. This field will ultimately

be the only dynamical field, which must be stored in computer memory and will represent the "lattice configuration" of the system.

One final remark must be made. Simulations based on Eq. (35) suffer from a severe technical problem, due to the fact that ϕ is a noncompact field. While the expression is formally correct, the determinant implicitly contains powers of ϕ up to ϕ^N, where N is the number of lattice sites. This causes numerical instabilities due to an uncontrollable amplification of rounding errors (in fact, we have previously verified this explicitly [27]). A solution to this problem was also worked out in Ref. [23] already, where it was shown that one can make the replacement

$$
-\delta_{xy}\delta_{t-1,t'} + \frac{\beta}{N_t}\frac{V_{xx}}{2}\delta_{xy}\delta_{t-1,t'} + i\frac{\beta}{N_t}\phi_{x,t}\delta_{xy}\delta_{t-1,t'}
$$

$$
\longrightarrow -e^{-i\frac{\beta}{N_t}\phi_{x,t}}\delta_{xy}\delta_{t-1,t'}, \tag{38}
$$

which introduces a compact field that is numerically stable (the determinant then contains sums over ϕ rather than products). The argument presented in Ref. [23] is based on the observation that the fermionic part of the Hubbard-Stratonovich transformed action corresponding to the path integral in Eq. (36) in the temporal continuum limit $\delta \to 0$

becomes invariant under spatially constant one-dimensional (temporal) gauge transformations. This gauge invariance is maintained in the discretized version when the compact field is used as a parallel transporter between time slices in the fermion matrix. The two discretizations are equivalent in the continuum limit. An alternative way to see this is to apply the Hubbard-Stratonovich transformation directly on the operator level rather than the field level, i.e., in the form

$$\exp\left(-\frac{\delta}{2}\sum_{x,y}q_x V_{xy}q_y\right)$$

$$\propto \int \left(\prod_x \phi_x\right)\exp\left(-\frac{\delta}{2}\sum_{x,y}\phi_x V_{xy}^{-1}\phi_y - i\,\delta\sum_x \phi_x q_x\right),$$
(39)

already in Eq. (26). Rather than using Eq. (23) for the normal ordered form of the interaction on the left-hand side, one then computes the matrix elements of the last term on the right containing the charge operator q_x using that [26]

$$\langle\xi|\,e^{\sum_{x,y}a_x^\dagger A_{xy}a_y}\,|\xi'\rangle = \exp\left[\sum_{x,y}\xi_x^*\left(e^A\right)_{xy}\xi'_y\right], \qquad (40)$$

which holds for arbitrary matrices A. Here, A is a diagonal matrix with elements $A_{xx} = \pm i\delta\,\phi_x$. One then obtains the fermion operator directly as

$$M_{(x,t)(y,t')} = \delta_{xy}(\delta_{tt'} - e^{-i\frac{\beta}{N_t}\phi_{x,t}}\delta_{t-1,t'})$$
$$- \kappa\frac{\beta}{N_t}\sum_{\vec{n}}\delta_{y,x+\vec{n}}\delta_{t-1,t'} + m_s\frac{\beta}{N_t}\delta_{xy}\delta_{t-1,t'},$$
(41)

in which $\exp(-i\frac{\beta}{N_t}\phi_{x,t})$ acts as the parallel transporter in the Euclidean time direction.

C. The hybrid Monte Carlo algorithm

Our principal objective is to compute expressions of the form

$$\langle O\rangle = \int \mathcal{D}\phi\, O(\phi)P(\phi), \qquad (42)$$

where

$$P(\phi) = \frac{1}{Z}\det[M(\phi)M^\dagger(\phi)]e^{-S(\phi)}. \qquad (43)$$

Here, ϕ is the Hubbard-Coulomb field introduced in the preceding section,[3] $O(\phi)$ is some function of this field, which represents an observable, $S(\phi)$ is the part of the action which depends on ϕ only, and $\det(MM^\dagger)$ accounts for the effects of

the fermions. This problem is precisely of the form, which is encountered in lattice gauge theory, where one has fermionic degrees of freedom (usually quark fields) interacting via gauge fields. Here we only have the scalar field ϕ, which represents the partially screened Coulomb field as the zero component of the Abelian photon field in the instantaneous approximation.

The Monte Carlo approach to the problem is to generate representative configurations of the field ϕ with probability $P(\phi)$ and measure observables $O(\phi)$ on these configurations. A well-established algorithm to generate these configurations is the hybrid Monte Carlo algorithm [45–47]. The first step is to represent the fermion determinant as a Gaussian integral over pseudofermion fields χ (these are commuting complex field variables rather than Grassmann numbers) using Eq. (31) with the negative sign on the right-hand side. We thus obtain

$$\mathrm{Tr}\,e^{-\beta H} = \int \mathcal{D}\phi\,\mathcal{D}\chi\,\mathcal{D}\chi^* \exp\Bigg[-\frac{\delta}{2}\sum_{t=0}^{N_t-1}\sum_{x,y}\phi_{x,t}V_{xy}^{-1}\phi_{y,t}$$
$$- \sum_{t,t'=0}^{N_t-1}\sum_{x,x'}\chi_{x,t}^*(MM^\dagger)_{(x,t)(x',t')}^{-1}\chi_{x',t'}\Bigg]. \qquad (44)$$

Note that the inverse of $MM^\dagger$ now appears in the exponent.[4]

Now that we have introduced the pseudofermions, we are faced with the problem of generating ϕ,χ according to a joint probability density

$$P(\phi,\chi) = \frac{1}{Z}e^{-S(\phi)-S'(\chi)}. \qquad (45)$$

The way to approach this problem is to generate ϕ and χ separately. One combines a heat-bath update of the pseudofermions (the distribution of χ thus is generated "directly" as $P(\chi)\sim e^{-\chi^\dagger(MM^\dagger)^{-1}\chi}$) with a molecular dynamics (MD) evolution of the Hubbard-Coulomb field. The MD evolution is a fictitious dynamical process, which evolves the field ϕ in computer time τ from some starting configuration in such a way that, after a suitable thermalization time, the propagation through phase space is consistent with the distribution defined by Eq. (45). It is generated by introducing a fictitious momentum field π associated with the τ evolution of ϕ. This then defines a Hamiltonian $\mathcal{H} = S(\phi) + S'(\chi) + \frac{\pi^2}{2}$ [which implies that π is distributed as $P(\pi)\sim e^{-\pi^2/2}$]. The Hubbard field ϕ is allowed to evolve by integrating Hamilton's equations for ϕ and π.

Since the equations cannot be solved exactly a symplectic integrator such as the Leapfrog integrator is used (discussed below), which introduces an error (difference in energy $\Delta\mathcal{H}$) from the finite step-sizes used in such integrators. This is then corrected by performing a Metropolis check at the end of each trajectory. The complete hybrid Monte Carlo (HMC) algorithm

---

[3]Note that we have suppressed the indices here, i.e. $\phi_{x,t}\equiv\phi$. ϕ is then understood as denoting a vector whose components are labeled by space-time indices. Where appropriate, we use such short-hand notation in the following for the Hubbard-Coulomb field as well as the pseudofermion fields. Analogously, we use a vector/matrix notation for quadratic forms such as $\sum_{i,j}\chi_i^* A_{ij}\eta_j \equiv \chi^\dagger A\eta$ where i,j label all pairs (x,t).

[4]Since $MM^\dagger$ is a positive Hermitian matrix, given a complex source vector A one can efficiently compute $B = (MM^\dagger)^{-1}A$ using the conjugate gradient algorithm. For an excellent (unpublished) pedagogical presentation see *An Introduction to the Conjugate Gradient Method Without the Agonizing Pain* by J. Shewchuk which can be found on the website of the author.

thus consists of repeating the following steps: (1) update the momentum field π using Gaussian noise: $P(\pi) \sim e^{-\pi^2/2}$; (2) update pseudofermions χ by generating another complex field ρ with $P(\rho) = e^{-\rho^\dagger \rho}$ and then obtaining $\chi = M\rho$; (3) generate a molecular dynamics trajectory; and (4) perform Metropolis check to correct step-size error: accept new configuration with probability $P = \min(1, e^{-\Delta\mathcal{H}})$.

For the reminder of this section, we will discuss the details of the MD evolution, which is the central part of the algorithm. Consider that we have introduced the momentum field π. We thus have the Hamiltonian

$$\mathcal{H} = \frac{\delta}{2} \sum_{t=0}^{N_t-1} \sum_{x,y} \phi_{x,t} V_{xy}^{-1} \phi_{y,t}$$
$$+ \sum_{t,t'=0}^{N_t-1} \sum_{x,x'} \chi_{x,t}^* (MM^\dagger)_{(x,t)(x',t')}^{-1} \chi_{x',t'} + \frac{1}{2} \sum_{t=0}^{N_t-1} \sum_x \pi_{x,t}^2. \tag{46}$$

In vector/matrix notation, this assumes the compact form:

$$\mathcal{H} = \frac{\delta}{2} \phi^T V^{-1} \phi + \chi^\dagger (MM^\dagger)^{-1} \chi + \frac{\pi^T \pi}{2}. \tag{47}$$

Hamilton's equation are then given by

$$\left[\frac{d\phi}{d\tau}\right]^T = \frac{\partial\mathcal{H}}{\partial\pi}, \quad \left[\frac{d\pi}{d\tau}\right]^T = -\frac{\partial\mathcal{H}}{\partial\phi}. \tag{48}$$

Given a set of initial conditions (ϕ, π), solutions to this set of equations can be approximated numerically using Leapfrog integration: assume that the time derivatives are approximated by finite differences

$$\frac{d\phi}{d\tau} \approx \frac{1}{\epsilon}[\phi(\tau+\epsilon) - \phi(\tau)] \equiv \frac{1}{\epsilon}(\phi_{\tau+1} - \phi_\tau),$$
$$\frac{d\pi}{d\tau} \approx \frac{1}{\epsilon}[\pi(\tau+\epsilon) - \pi(\tau)] \equiv \frac{1}{\epsilon}(\pi_{\tau+1} - \pi_\tau). \tag{49}$$

We then define position steps $V_\phi(\epsilon)$ and momentum steps $V_\pi(\epsilon)$ as

$$V_\phi(\epsilon): \quad \phi_{\tau+1} = \phi_\tau + \epsilon(\partial\mathcal{H}/\partial\pi)^T,$$
$$V_\pi(\epsilon): \quad \pi_{\tau+1} = \pi_\tau - \epsilon(\partial\mathcal{H}/\partial\phi)^T. \tag{50}$$

Leapfrog integration consists of iterating combinations of steps of the form

$$V_\pi(\epsilon/2)V_\phi(\epsilon)V_\pi(\epsilon/2) \quad \text{or} \quad V_\phi(\epsilon/2)V_\pi(\epsilon)V_\phi(\epsilon/2) \tag{51}$$

until a desired trajectory length $L = N\epsilon$ is reached. The former is known as PQP integration, the latter as QPQ integration. Leapfrog integration does not conserve energy. The error (deviation from the "true" trajectory through phase space) can be quantified by the difference in energy $\Delta\mathcal{H}$ and is of order $\Delta\mathcal{H} \sim \mathcal{O}(\epsilon^2)$.

To derive the expressions for the derivatives of $\mathcal{H}$, we use matrix calculus. We assume a numerator convention, i.e., vectors ρ, σ, which are defined as columns, and derivatives,

which are defined as

$$\frac{d\sigma}{d\rho} = \begin{pmatrix} \frac{\partial\sigma_1}{\partial\rho_1} & \cdots & \frac{\partial\sigma_1}{\partial\rho_n} \\ \vdots & \ddots & \vdots \\ \frac{\partial\sigma_m}{\partial\rho_1} & \cdots & \frac{\partial\sigma_m}{\partial\rho_n} \end{pmatrix}, \quad \frac{dM}{ds} = \begin{pmatrix} \frac{\partial M_{11}}{\partial s} & \cdots & \frac{\partial M_{1m}}{\partial s} \\ \vdots & \ddots & \vdots \\ \frac{\partial M_{n1}}{\partial s} & \cdots & \frac{\partial M_{nm}}{\partial s} \end{pmatrix},$$

$$\frac{d\sigma}{ds} = \begin{pmatrix} \frac{\partial\sigma_1}{\partial s} \\ \vdots \\ \frac{\partial\sigma_m}{\partial s} \end{pmatrix}, \quad \frac{ds}{d\rho} = \left(\frac{\partial s}{\partial\rho_1}, \ldots, \frac{\partial s}{\partial\rho_n}\right), \tag{52}$$

where s is a scalar and M is a matrix. The following identities then hold:

$$\frac{d(\sigma^T \sigma)}{d\rho} = 2\sigma^T \frac{d\sigma}{d\rho},$$

$$\frac{d(\rho^T A\rho)}{d\rho} = 2\rho^T A, \quad \frac{dU^{-1}}{ds} = -U^{-1}\frac{dU}{ds}U^{-1}, \tag{53}$$

$$\frac{d(UV)}{ds} = U\frac{dV}{ds} + \frac{dU}{ds}V.$$

Here, U and V are matrices that depend on s, and A is a symmetric matrix that does not depend on ρ.

It is now easy to see that

$$\left[\frac{d\phi}{d\tau}\right]^T = \frac{\partial\mathcal{H}}{\partial\pi} = \pi^T. \tag{54}$$

The second equation requires a little more work. It consists of two terms, which are the force terms generated by the Hubbard-Coulomb and the fermion fields. Using the above identities, it follows that

$$\left[\frac{d\pi}{d\tau}\right]^T = -\frac{\partial\mathcal{H}}{\partial\phi}$$
$$= -\delta\phi^T V^{-1} - \frac{\partial}{\partial\phi}[\chi^\dagger(MM^\dagger)^{-1}\chi] \equiv F_\phi + F_\chi. \tag{55}$$

Deriving the Hubbard force F_ϕ was straightforward. To obtain the fermion force F_χ, we note that it is vector valued. It can be evaluated component-wise as

$$(F_\chi)_k = -\frac{\partial}{\partial\phi_k}[\chi^\dagger(MM^\dagger)^{-1}\chi]$$
$$= -\chi^\dagger\left[\frac{\partial(MM^\dagger)^{-1}}{\partial\phi_k}\right]\chi$$
$$= \chi^\dagger(MM^\dagger)^{-1}[\frac{\partial(MM^\dagger)}{\partial\phi_k}](MM^\dagger)^{-1}\chi$$
$$= \chi^\dagger(MM^\dagger)^{-1}\left(\frac{\partial M}{\partial\phi_k}M^\dagger + M\frac{\partial M^\dagger}{\partial\phi_k}\right)(MM^\dagger)^{-1}\chi$$
$$= \eta^\dagger\frac{\partial M}{\partial\phi_k}\xi + \xi^\dagger\frac{\partial M^\dagger}{\partial\phi_k}\eta$$
$$= 2\,\mathrm{Re}\left(\eta^\dagger\frac{\partial M}{\partial\phi_k}\xi\right). \tag{56}$$

Here we have introduced the notation

$$\eta = (MM^\dagger)^{-1}\chi, \quad \xi = M^{-1}\chi = M^\dagger\eta. \tag{57}$$

The precise form of the fermion force now depends on the choice of M. For the fermion-matrix defined in Eq. (35), we obtain

$$(F_\chi)_{(x,t)} = -\frac{\partial}{\partial\phi_{(x,t)}}[\chi^\dagger(MM^\dagger)^{-1}\chi]$$

$$= -2\frac{\beta}{N_t}\mathrm{Im}[\eta^*_{(x,t)}\xi_{(x,t-1)}]. \qquad (58)$$

For the version, which uses the compact Hubbard field [with the substitution as shown in Eq. (38)], we obtain

$$(F_\chi)_{(x,t)} = -\frac{\partial}{\partial\phi_{(x,t)}}[\chi^\dagger(MM^\dagger)^{-1}\chi]$$

$$= -2\frac{\beta}{N_t}\mathrm{Im}[\eta^*_{(x,t)}e^{-i\frac{\beta}{N_t}\phi_{x,t}}\xi_{(x,t-1)}]. \qquad (59)$$

Lastly, it should be pointed out that it is often possible to choose a numerical integration scheme, which performs better than the standard Leapfrog integration defined in Eq. (51). In particular, when the force $F = d\pi/d\tau$ is, as is the case here, composed of different components F_i, which differ both in magnitude and associated computational cost, one may obtain a more efficient integrator by decomposing the momentum steps $V_\pi(\epsilon)$ into substeps $V_\pi^{F_i}(\epsilon)$, which each use only one of the force components. If, for example, one has $F = F_1 + F_2$, where F_2 is both much cheaper to compute and of larger magnitude than

F_1, one may gain performance by using the decomposition

$$V_\pi(\epsilon) \to V_\pi^{F_1}(\epsilon/2)\left[V_\pi^{F_2}(\epsilon/m)\right]^m V_\pi^{F_1}(\epsilon/2). \qquad (60)$$

This is known as Sexton-Weingarten integration [48]. The constant m must be tuned to the particular problem. It is often (but not always) a good idea to tune m such that the force components entering into Eq. (60) are of a similar magnitude.

D. The order parameter

We wish to investigate spontaneous breaking of sublattice symmetry. Thus we require a proper order parameter as determined by the mass term which acts as the explicitly symmerty breaking external field. The corresponding choice here is to use the difference of the spin density operators on the two sublattices A and B,

$$\Delta_N = n_A - n_B$$

$$= \frac{1}{L_x L_y}\left[\sum_{x\in X_A}(a_x^\dagger a_x + b_x^\dagger b_x) - \sum_{x\in X_B}(a_x^\dagger a_x + b_x^\dagger b_x)\right]. \qquad (61)$$

Its expectation value is given by

$$\langle\Delta_N\rangle = \frac{1}{Z}\mathrm{Tr}(\Delta_N e^{-\beta H}), \qquad (62)$$

which in the functional integral form is expressed as

$$\langle\Delta_N\rangle = \frac{1}{ZN_tL_xL_y}\int\mathcal{D}\psi\,\mathcal{D}\psi^*\,\mathcal{D}\eta\,\mathcal{D}\eta^*\left[\sum_{X_A,t}(\psi^*_{x,t+1}\psi_{x,t} + \eta^*_{x,t+1}\eta_{x,t}) - \sum_{X_B,t}(\psi^*_{x,t+1}\psi_{x,t} + \eta^*_{x,t+1}\eta_{x,t})\right]e^{-\beta H}$$

$$= \frac{-1}{\beta ZL_xL_y}\frac{\partial}{\partial m}\int\mathcal{D}\psi\,\mathcal{D}\psi^*\,\mathcal{D}\eta\,\mathcal{D}\eta^*\,e^{-\beta H} = \frac{-1}{\beta ZL_xL_y}\int\mathcal{D}\phi\left[\frac{\partial}{\partial m}\det(MM^\dagger)\right]e^{-S[\phi]}$$

$$= \frac{-1}{\beta ZL_xL_y}\int\mathcal{D}\phi\,\det(MM^\dagger)\mathrm{Tr}\left[M^{-1}\frac{\partial(MM^\dagger)}{\partial m}M^{-1\dagger}\right]e^{-S[\phi]}$$

$$= \frac{-2}{\beta ZL_xL_y}\int\mathcal{D}\phi\,\det(MM^\dagger)\mathrm{ReTr}\left(M^{-1}\frac{\partial M}{\partial m}\right)e^{-S[\phi]}. \qquad (63)$$

As the magnetization in a classical spin system, it is of course given by the derivative with respect to the external field. Using Eq. (35), we then obtain

$$\langle\Delta_N\rangle = \frac{-2}{N_tL_xL_y}\sum_{t=0}^{N_t-1}\mathrm{Re}\left\langle\sum_{x\in X_A}M^{-1}_{(x,t)(x,t+1)} - \sum_{x\in X_B}M^{-1}_{(x,t)(x,t+1)}\right\rangle. \qquad (64)$$

This expression is very similar to the lattice formulation of the chiral condensate in QCD. It holds for both, compact and noncompact Hubbard-Coulomb fields.

Computing this order parameter hence amounts to computing the expectation value of a trace of an operator, i.e.,

$$\langle\Delta_N\rangle = \mathrm{Re}\langle\mathrm{Tr}(D^{-1})\rangle, \qquad (65)$$

with D defined appropriately. Straightforward calculation of such a trace is not feasible. A widely used method to deal with this problem is the noisy estimator approach (see, e.g., Ref. [47]). Using Gaussian noise vectors, i.e., complex pseudofermion sources χ randomly drawn from $P(\chi)\sim\exp(-\chi^\dagger\chi)$, one can estimate the trace (on a given

lattice configuration) as

$$\mathrm{Tr}(D^{-1}) \approx \frac{1}{K}\sum_{k=1}^{K}\chi^{(k)\dagger}D^{-1}\chi^{(k)}. \qquad (66)$$

Here, K is the total number or source vectors and k is the index, which labels them. The accuracy of the estimate becomes successively better with increasing K.

E. Second-order fermion operator

Equation (35) is by far not the only possible form for the fermion matrix. As was discussed in Ref. [23], there is a great amount of freedom in discretizing the Euclidean time
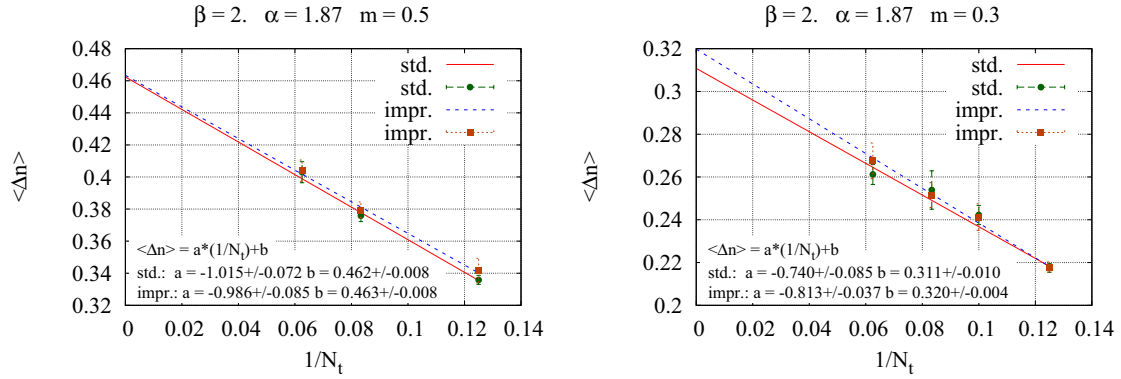
FIG. 2. (Color online) Comparison of $1/N_t$ scaling of $\langle \Delta_N \rangle$ on $L_x = L_y = 6$ lattices. The first- and second-order discretizations are referred to as "std." and "impr.," respectively, in the figures. The potential chosen for these simulations includes the effect of mirror charges and is discussed in Ref. [27].

direction which could, in principle, be exploited to construct improved actions that approach the continuum limit faster. A particular second-order discretization scheme was proposed in Ref. [26]. We have previously obtained some evidence (on small lattices and with a potential, which differs from the one used in this work) that this version is, in terms of discretization errors affecting the order parameter, equivalent to the direct discretization discussed in the preceding paragraph and does not yield any improvement. In Fig. 2, we show two examples. See Ref. [27] for further details. An extensive autocorrelation analysis has not yet been done, but would be useful to determine whether there is any performance gain. In any case, for the purpose of cross-checking our results we have implemented this version in our code also. We sketch the derivation in this section. In particular,

we highlight which aspects of the preceding discussions are changed.

Consider that we have introduced coherent states and derived Eq. (26). At this point, one may choose to factor the exponential in such a way that the interacting part is split off,

$$e^{-\delta H} = e^{-\delta(H_c + H_{tb} + H_m)} \rightarrow e^{-\delta(H_{tb} + H_m)} e^{-\delta H_c}. \qquad (67)$$

We insert an additional set of coherent states between the factors and relabel all states to restore the lexicographic ordering of their index (in fact, compared to previously, the enumeration of the t coordinate is reversed in order to match the conventions of Ref. [26], but this is of no further relevance since it is a trivial relabeling). We then obtain

$$\text{Tr}\, e^{-\beta H} = \int \left(\prod_{t=0}^{2N_t - 1} \prod_x d\psi_{x,t}^* d\psi_{x,t} d\eta_{x,t}^* d\eta_{x,t} \right) \prod_{t=0}^{N_t - 1} \exp\left[-\sum_x (\psi_{x,2t}^* \psi_{x,2t} + \eta_{x,2t}^* \eta_{x,2t} + \psi_{x,2t+1}^* \psi_{x,2t+1} + \eta_{x,2t+1}^* \eta_{x,2t+1}) \right]$$

$$\times \langle \psi_{2t}, \eta_{2t} | e^{-\delta(H_{tb} + H_m)} | \psi_{2t+1}, \eta_{2t+1} \rangle \langle \psi_{2t+1}, \eta_{2t+1} | e^{-\delta H_c} | \psi_{2t+2}, \eta_{2t+2} \rangle. \qquad (68)$$

Computing the matrix elements and introducing the compact Hubbard-Coulomb field as previously now yields

$$\text{Tr}\, e^{-\beta H} = \int \left(\prod_{t=0}^{2N_t - 1} \prod_x d\psi_{x,t}^* d\psi_{x,t} d\eta_{x,t}^* d\eta_{x,t} \right) \left(\prod_{t=0}^{N_t - 1} \prod_x d\phi_{x,t} \right) e^{-(S_\psi + S_\eta)} \exp\left(-\frac{\delta}{2} \sum_{t=0}^{N_t - 1} \sum_{x,y} \phi_{x,t} V_{xy}^{-1} \phi_{y,t} \right), \qquad (69)$$

where we have

$$S_\psi = \sum_{t=0}^{N_t - 1} \left[\sum_x \psi_{x,2t}^* (\psi_{x,2t} - \psi_{x,2t+1}) - \delta\kappa \sum_{\langle x,y \rangle} (\psi_{x,2t}^* \psi_{y,2t+1} + \psi_{y,2t}^* \psi_{x,2t+1}) \right.$$

$$\left. + \sum_x \psi_{x,2t+1}^* (\psi_{x,2t+1} - e^{-i\delta\phi_{x,t}} \psi_{x,2t+2}) + \delta \sum_x m_s \psi_{x,2t}^* \psi_{x,2t+1} \right], \qquad (70)$$

and an analogous expression for S_η with the opposite charge, i.e., with a phase factor $e^{i\delta\phi_{x,t}}$. By introducing a fermion matrix of the form

$$M_{(x,t)(y,t')} = \begin{cases} \delta_{xy}(\delta_{tt'} - \delta_{t+1,t'}) - \frac{\beta}{N_t}\kappa \sum_{\vec{n}} \delta_{y,x+\vec{n}} \delta_{t+1,t'} + \frac{\beta}{N_t} m_s \delta_{xy} \delta_{t+1,t'} & : t \text{ even,} \\ \delta_{xy}\delta_{tt'} - \delta_{xy}\delta_{t+1,t'} \exp\left(-i\frac{\beta}{N_t}\phi_{x,(t-1)/2}\right) & : t \text{ odd,} \end{cases} \qquad (71)$$

we can then rewrite the fermionic component of the action as

$$S_F = S_\psi + S_\eta = \sum_{t,t'=0}^{2N_t - 1} \sum_{x,y} (\psi_{x,t}^* M_{(x,t)(y,t')} \psi_{y,t'} + \eta_{x,t}^* M_{(x,t)(y,t')}^* \eta_{y,t'}). \qquad (72)$$

Note that the Hubbard-Coulomb field appears only on odd time slices here. It hence follows that in HMC simulations, the pseudofermion fields have twice as many components as the Hubbard-Coulomb field. Rederiving the fermion force [Eq. (59)] for the second-order action is straightforward and yields

$$(F_\chi)_{(x,t)} = -2\frac{\beta}{N_t}\text{Im}\big[\eta^*_{(x,2t+1)}e^{-i\frac{\beta}{N_t}\phi_{x,t}}\xi_{(x,2t+2)}\big]. \qquad (73)$$

Likewise, the order parameter for sublattice symmetry breaking is computed as

$$\langle\Delta_N\rangle = \frac{-2}{N_t L_x L_y}\sum_{t=0}^{N_t-1}\text{Re}\left\langle\sum_{x\in x_A}M^{-1}_{(x,2t+1)(x,2t)}\right.$$
$$\left. - \sum_{x\in x_B}M^{-1}_{(x,2t+1)(x,2t)}\right\rangle. \qquad (74)$$

F. The partially screened Coulomb potential

We now turn to the interaction matrix V, which appears in the Hamiltonian and thus in the Hubbard action

$$S_\phi = \frac{\delta}{2}\sum_{t=0}^{N_t-1}\sum_{x,x'}\phi_{x,t}V^{-1}_{xx'}\phi_{x',t}. \qquad (75)$$

Note that we have absorbed the factor of e^2 ($= \alpha$ in our natural units) in the definition of the matrix V here. Also note that it is the *bare* coupling constant $\alpha \approx 1/137$ that enters into V, not the effective coupling constant $\alpha_{\text{eff}} = \alpha/v_F \approx 300/137$ (with $v_f = 3\kappa a/2$, i.e., the interaction strength relative to the kinetic energy as described by the free hopping Hamiltonian H_{tb}). In the simulations, we will account for dielectric screening by a substrate through rescaling of the charge $e^2 \to e^2/\epsilon$ and hence of the potential. We discuss our results both in terms of ϵ and in terms of the correspondingly screened *effective* fine-structure constant $\alpha_{\text{eff}} = \alpha_{\text{eff},0}/\epsilon \approx 2.2/\epsilon$.

It is clear that all results will depend, perhaps strongly, on the the two-body potential which is used and that ultimately the validity of the entire study depends on making physically sound assumptions about the exact form of V (the fact that the inverse of V appears will be addressed below). It is obvious that $V_{xx'}$ should depend only on the distance between the two lattice sites. Thus we have

$$V_{xx'} = V(x_1 - x'_1, x_2 - x'_2) \equiv V(r). \qquad (76)$$

The straightforward choice would be to assume that $V(r)$ is essentially a standard Coulomb potential $V(r) = e^2/r$, with a short-distance cutoff on the order of half a lattice spacing (as discussed in Refs. [23,24]).

It turns out, however, that this is insufficient to account for the short-distance screening by the electrons in the σ bands of graphene and other higher energy states. To obtain a quantitatively more accurate description of the partially screened Coulomb interactions, we use the results of Ref. [35] where this screening was investigated within a constrained random phase approximation (cRPA). In particular, we use the numerical values from this reference for the effective strengths of the on-site repulsion ($U_{00} = V_{xx}$), the nearest-neighbor ($U_{01} = V_{xx'}$ with $|x - x'| = a$), next-nearest-neighbor ($U_{02} = V_{xx'}$ with $|x - x'| = \sqrt{3}a$), and third-nearest-neighbor

($U_{03} = V_{xx'}$ with $|x - x'| = 2a$) interactions, which are given by

	U_{00} (eV)	U_{01} (eV)	U_{02} (eV)	U_{03} (eV)
cRPA	9.3	5.5	4.1	3.6

This part of the short-distance screening was implemented in Ref. [26] as well already. For larger distances, however, it was then simply assumed that the potential continues to fall off like $V(r) = e^2/(r\,\epsilon_0)$, with the constant ϵ_0 fixed to $\epsilon_0 = 1.41$ so as to match $V(2a)$ to U_{03}.

As mentioned in the introduction already, there is no screening of the long-range Coulomb tails in graphene, however. In order to describe the screening from the σ bands and other localized electron states we therefore use a phenomenological model $\epsilon_\sigma(\vec{k})$ that describes a thin film of thickness d with a dielectric screening constant ϵ_1. This model was adapted for graphene by placing the two-dimensional sheet in the middle of the film in Ref. [35] where it was found that an excellent fit to the computed cRPA dielectric screening at longer wavelengths is obtained for

$$\epsilon_\sigma^{-1}(\vec{k}) = \frac{1}{\epsilon_1}\frac{\epsilon_1 + 1 + (\epsilon_1 - 1)e^{-kd}}{\epsilon_1 + 1 - (\epsilon_1 - 1)e^{-kd}}, \qquad (77)$$

with $\epsilon_1 = 2.4$ and $d = 2.8$ Å ($\approx 1.41 \times 10^{-3}$ eV^{-1}). This model smoothly connects the explicit short-distance screening with the unscreened long-wavelength limit as $\epsilon_\sigma(\vec{k}) \to 1$ for $k \to 0$.

In order to obtain the corresponding partially-screened Coulomb interaction matrix $V_{xx'} = V(r)$, first consider the unscreened potential $V_0(r) = e^2/r$ in two spatial dimensions, which in momentum space reads $\widetilde{V}_0(\vec{k}) = (2\pi e^2)/k$. The partially screened $V(\vec{r})$ is then obtained by the inverse Fourier transform with the dielectric screening function $\epsilon_\sigma(\vec{k})$ from Eq. (77) included,

$$V(\vec{r}) = \frac{1}{(2\pi)^2}\int_{\mathbb{K}^2}d^2k\,\widetilde{V}_0(\vec{k})\,\epsilon_\sigma^{-1}(\vec{k})\,e^{-i\vec{k}\vec{r}}$$
$$= e^2\int_0^\infty dk\,\epsilon_\sigma^{-1}(\vec{k})\,J_0(kr), \qquad (78)$$

where $J_0(x)$ is a Bessel function of the first kind. The remaining one-dimensional and well-behaved integral can be easily computed numerically. Figure 3 shows a comparison between the standard Coulomb potential, the potential used in Ref. [26] (referred to as "ITEP screened potential" in the following) and the result obtained from Eq. (78) (referred to as "partially screened Coulomb potential"). It can be seen that the result from Eq. (78) indeed connects with the explicit cRPA values at short distances and smoothly approaches the unscreened Coulomb potential at large distances.

For portability, and to gain a better understanding how relevant screening is on different length scales, we have parametrized $V(r)$. It turns out that an ansatz, which assumes exponential (Debye) screening, works well, provided that the mass (inverse screening length) is allowed to depend on the length scale. Ultimately, for simulations, we use a piecewise
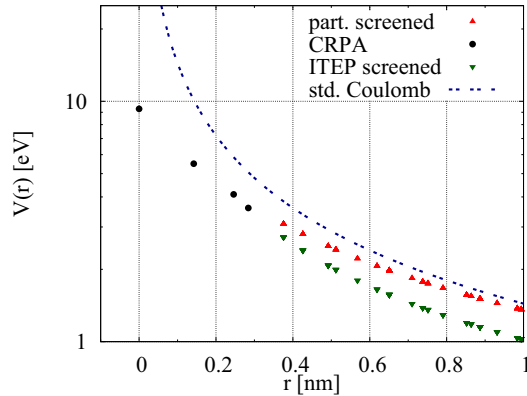
FIG. 3. (Color online)   Comparison of the unscreened Coulomb potential (dashed blue), the short-distance cRPA results of Ref. [35] (black), the long-range parts with constant ϵ_0 to match U_{03} as in Ref. [26] (green), and the long-range parts from the phenomenological screening formula of Ref. [35] with unscreened Coulomb tails (red).

defined potential

$$
V(r) = \begin{cases} U_{00}, U_{01}, U_{02}, U_{03}, & r \leqslant 2a \\ e^2([\exp(-m_2 r)/(m_1 r)^\gamma]m_0 + m_3), & r > 2a \end{cases},
$$

(79)

where a is the lattice spacing, $m_1 = 1$ eV, and the parameters m_0, γ, m_2, m_3 differ depending on the length-scale as is summarized in the following table:

	m_0 (eV)	γ	m_2 (eV)	m_3 (eV)
$8a \geqslant r > 2a$	9.0380311	0.632469	144.354	62.41496
$30a \geqslant r > 8a$	2.0561977	0.862664	27.8362	15.29088
$120a \geqslant r > 30a$	1.03347891	0.990975	0.0	−0.134502
$r > 120a$	1.0	1.0	0.0	0.0

We find that using these values our ansatz differs from the numerical results from Eq. (78) by no more than ∼0.1% for any r and hence is sufficiently accurate for our purposes. Furthermore, these parameters show that while there is rather strong screening for $r < 8a$, the Coulomb potential remains essentially unscreened for $r > 30a$.

Since in the simulation we want to maintain translational invariance in order to minimize boundary effects, we have to make the Coulomb interaction also translationally invariant. A naive sum over infinitely many mirror charges with the long-range $1/r$ interaction would not converge. In order to restore translational invariance in the interaction while keeping the physical infrared cutoff that is set by the size of a finite graphene sheet at the same time, we choose to account for the boundary conditions in the following way: for any two points x and x' on the lattice, we determine the shortest path between these points, which can be constructed if boundary crossings are allowed. The matrix element $V_{xx'}$ is then the potential $V(r)$ associated with this path. A potential constructed in such a way is translationally invariant, but does not introduce infrared

divergences. The natural infrared regulator is then given by the finite size of the sample.

In Eq. (75), the inverse of V appears. How to efficiently compute this expression is a non-trivial technical problem. Explicitly inverting V and storing the elements of V^{-1} requires large amounts of memory. Instead, what is currently done in our code is to use the conjugate gradient algorithm to invert V on a given source ϕ. This amounts to finding the solution η of

$$
\phi_{x,t} = \sum_{x'} V_{xx'} \eta_{x',t}.
$$

(80)

To do this, repeated computations of $V\eta$ are required. Since V depends on the distance only, formally this is a two-dimensional convolution (for fixed t), which suggests carrying out the computation in momentum space. If the matrix V is constructed as discussed above, always using the shortest path to determine $V(r)$, Eq. (80) can be brought into a form, which is exactly a cyclic convolution by introducing a rectangular fine-grid coordinate system as discussed in Sec. II A (the base vectors then coincide with the axes of periodicity): we introduce fields ϕ' and η' on the fine grid. The former has the same value as ϕ on those points which are occupied by a carbon atom, and is zero on all other points. Likewise, we introduce a matrix V' over the fine grid which contains V_{x0} at each point. We then obtain $\tilde{\phi}'_{k,t}$ (only the space-index is transformed) and $\tilde{V}'_k$ in this coordinate system using the CUDA fast Fourier transform (cuFFT) library. ϕ in Eq. (80) is then equal to the inverse Fourier transform of the pointwise product of $\tilde{V}'_k$ and $\tilde{\eta}'_{k,t}$, restricted to the points that coincide with points on the hexagonal lattice.

Note that we have first obtained the screened potential $V(r)$ by numerically integrating Eq. (78) *in the continuum and infinite volume*. From this, the discretized matrix V is constructed. The discretized $\tilde{V}'_k$ for the finite periodic lattice is then obtained from this result. This procedure is free of additional sources of discretization and finite volume errors, which would enter if one instead applied screening via $\epsilon_\sigma^{-1}(\vec{k})$ to a discretized $\tilde{V}'_k$, which was obtained from an unscreened matrix V.

Unfortunately, it is not (at least not trivially) possible to compute the inverse of V directly in momentum space by doing pointwise divisions of $\tilde{\phi}'_{k,t}$ and $\tilde{V}'_k$. This is due to the additional spatial points of the fine grid, which do not correspond to a site on the hexagonal lattice.

III. RESULTS

We simulate the interacting tight-binding theory via hybrid Monte Carlo for $L_x = L_y = 18$ and $N_t = 20$. We choose $\beta = 2.0$ eV^{-1} for the entire study. The reasoning behind this choice of β is the following. It was discussed in Ref. [20] that a temperature driven phase transition of the Berezinskii-Kosterlitz-Thouless type destroys sublattice symmetry breaking for high temperatures of the electron gas. In Ref. [25], the critical temperature separating the high- and low-temperature phases was estimated to be $T_c \approx 1.3 \times 10^4$ K (corresponding to $\beta \approx 0.89$ eV^{-1}). Subsequently, both Refs. [25] and [26] conducted simulations at $\beta = 2.0$ eV^{-1}, which corresponds to $T \approx 5.8 \times 10^3$ K, well below T_c. We adopt this choice to make a direct comparison possible. Ultimately, in order to
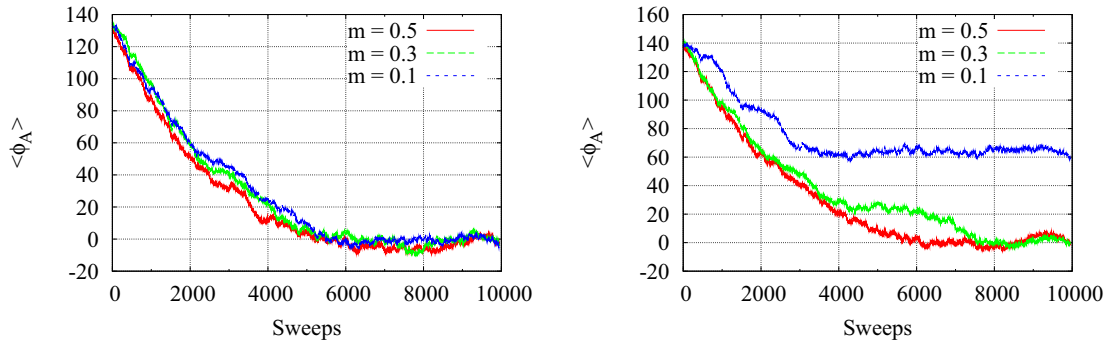
FIG. 4. (Color online) Thermalization of the ϕ field on sublattice A for an ordered start (ITEP-screened potential). (Left) $\epsilon = 0.5$ ($\alpha_{\text{eff}} \approx 4.379$). (Right) $\epsilon = 0.9$ ($\alpha_{\text{eff}} \approx 2.433$).

realistically account for finite temperature, lattice vibrations must also be included, which is beyond the scope of our present work.

Our first goal is to reproduce the results of Ref. [26]. We thus start by simulating the second-order fermion matrix using compact Hubbard field variables and construct a screened potential accordingly (constant screening at long distances, cRPA results at short distances). This is followed by a simulation of the partially screened potential. The first-order discretization scheme is then used.

For both cases, we choose different values for the rescaling factor ϵ in the range $\epsilon = 0.45$–1.0 (which in fact mostly lie outside of the physical region). This corresponds to values of the effective fine-structure constant α_{eff} in the range $\alpha_{\text{eff}} \approx 5.0$–$2.0$. For each choice of ϵ we simulate $m = 0.5, 0.4, 0.3, 0.2, 0.1$ eV. We use a Sexton-Weingarten multiscale integrator with two scales: the step-size for the Hubbard force is $\delta = 1.0$ and for the fermion force is $\delta/10 = 0.1$. The trajectory length is $L = 10$. We find that this yields satisfactory Metropolis acceptance rates of $\sim 2/3$ for each choice of m and ϵ. The number of conjugate gradient iterations required for inverting the fermion matrix strongly increases with decreasing mass. The smaller masses are thus substantially more expensive than the larger ones in terms of computer time.

We begin with investigating thermalization times. Regardless of the fact that the Hubbard-Coulomb field enters as a compact link variable in the fermion operator, it is a noncompact variable in the Hubbard action. This means that

unlike in theories with strictly compact field variables [e.g., SU(N) gauge theories], one can move arbitrarily far away from thermal equilibrium. The choice of proper starting conditions is therefore a nontrivial matter. It is complicated by the fact that acceptance rates are strongly reduced far from equilibrium.

For the first study (second-order fermion matrix, constant screening at long distances), we have done the following. For each set of parameters, we initialize the ϕ field by setting $\phi_{x,t} = 300$ for each (x,t). We then conduct 100 MD trajectories without a Metropolis check. This does not suffice to bring the system into equilibrium, but it brings the system into a region where Metropolis acceptance is reasonable. After these trajectories, we switch on the Metropolis check. In Fig. 4, it is shown how the ϕ field evolves on one sublattice (in this case sublattice A) over the $10k$ subsequent trajectories for $\epsilon = 0.5, 0.9$ ($\alpha_{\text{eff}} \approx 4.379, 2.433$) and $m = 0.1, 0.3, 0.5$ eV. Before taking measurements, we discard on the order of $10k$ trajectories for each combination of parameters. As the figure illustrates, at small coupling and $m = 0.1$ eV, this potentially introduces a systematic error due to incomplete thermalization (discarding two or three times as many trajectories does not help. $\langle \phi \rangle \approx 0.0$ is not reached, even after $\sim 30k$ trajectories). This issue has only affected the two smallest values of α_{eff}, which are simulated and leads to a slight overestimation of the order parameter in the $m \to 0$ limit. We further discuss this below.

For the simulations with the (correct) partially screened potential, we have revised our methodology and improved thermalization: we first conduct one run of $10k$ trajectories
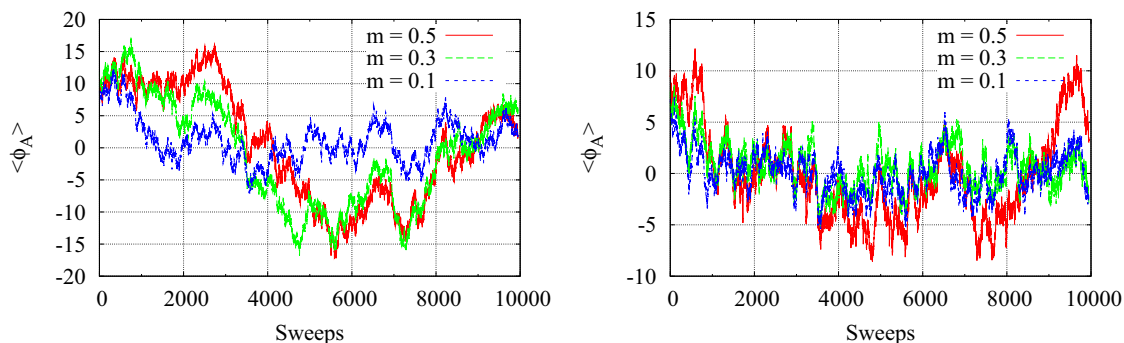

FIG. 5. (Color online) Thermalization of the ϕ field on sublattice A when using a prethermalized configuration of a different parameter set (partially screened potential). (Left) $\epsilon = 0.5$ ($\alpha_{\text{eff}} \approx 4.379$). (Right) $\epsilon = 0.9$ ($\alpha_{\text{eff}} \approx 2.433$) .
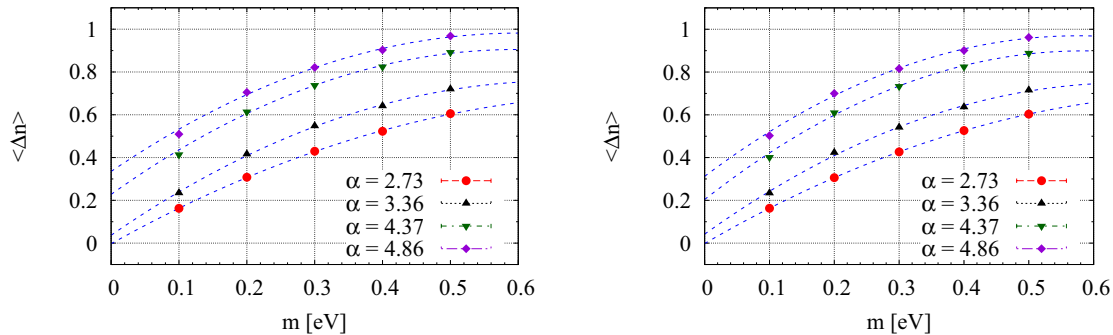
FIG. 6. (Color online) Examples of $m \to 0$ extrapolation of order parameter (error bars are smaller than points). (Left) Partially screened potential / first-order discretization. (Right) Constant screening at long-range/second-order discretization.

using the largest mass ($m = 0.5 \, \text{eV}$), which is cheap in terms of computer time. The final state of the ϕ field is then used as starting condition for all other runs. We again start with 100 trajectories without Metropolis checks. In Fig. 5, the subsequent $10k$ trajectories are shown, again for the $\alpha_{\text{eff}} \approx 4.379, 2.433$ and $m = 0.1, 0.3, 0.5$ eV. It appears that the system is already close to equilibrium after the 100 initial iterations. We discard another 1000 trajectories to be on the safe side.

For both versions, we measure the order-parameter for sublattice symmetry breaking $\langle \Delta_N \rangle$ using noisy estimators. Ten source vectors are used for each measurement. Measurements are done after every tenth MD trajectory. We measure on several hundreds of independent configurations (auto-correlations are estimated via binning) for each combination of α_{eff} and m. We extrapolate the results to the $m \to 0$ limit by doing a least squares fit to the form

$$\langle \Delta_N \rangle (m) = c_1 m^2 + c_2 m + c_3. \tag{81}$$

In Fig. 6, we show exemplary cases including the fit via Eq. (81). The figure shows both versions of the simulation (partially screened on the left and ITEP screened on the right). This figure already suggests a strong similarity between the two versions. In Fig. 7, we show the $m \to 0$ limiting cases for each α_{eff}. A strong similarity between the two different setups is observed. In fact, both results within errors cannot be distinguished from Ref. [26]. Our findings are consistent with a phase transition setting in around $\alpha_c \approx 3.14$. Note that for the two smallest values of α_{eff} we find $\langle \Delta_N \rangle$ slightly above

zero for the first setup, which is very likely a systematic error due to the incomplete thermalization discussed above.

IV. CONCLUSIONS AND OUTLOOK

In this work, we have conducted a hybrid Monte Carlo simulation of the interacting tight-binding model for a $18 \times 18 \times 20$ lattice with periodic boundary conditions. We have simulated the system using two different setups: (a) a second-order fermion matrix and a potential which is screened both at short and long distances, and (b) a first-order fermion matrix and a partially screened Coulomb potential.

We have investigated spontaneous breaking of sublattice symmetry in both cases. With our setup (a), we have demonstrated consistency with Ref. [26]. We confirm the result of these authors, who find that the phase transition occurs at $\alpha_c \approx 3.14$. With our setup (b), we have investigated how this result changes when the unscreened long-range Coulomb tails of the electronic interactions in graphene at half-filling are properly accounted for. We have demonstrated that the effect on the order parameter $\langle \Delta_N \rangle$ is small. We find, within errors, no difference between the two setups, for the entire range of α_{eff} which was considered. This result suggests that development of the band gap is insensitive to the long-distance part of the potential. It also confirms that screening of the interactions by electrons in the π orbitals may indeed be a mechanism, which explains the experimental finding that suspended graphene is a conductor.

For the future, it is immediately clear that these results should be extrapolated to both the infinite volume and the
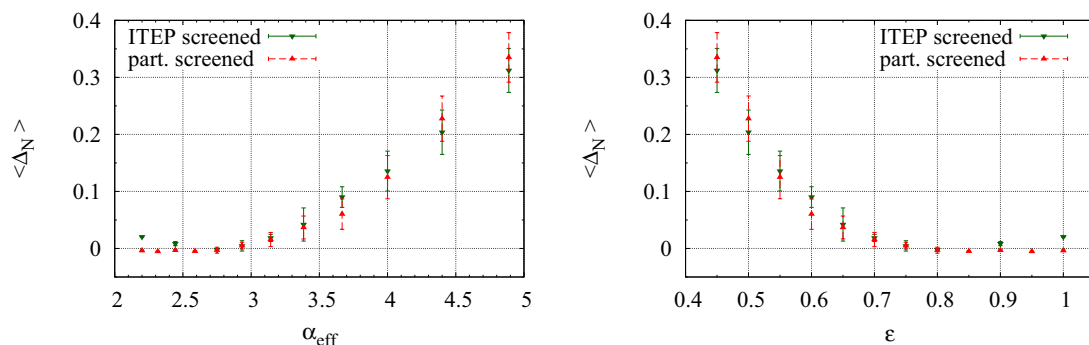

FIG. 7. (Color online) The $m \to 0$ extrapolated results for the order parameter Δ_N as a function of α_{eff} (left) and as a function of a rescaling parameter ϵ (right).

(timelike) continuum limit. In particular it will be interesting to see whether the long-distance behavior gets more important at larger volumes. Aside from this obvious extension of the investigation presented in this paper, there is a large number of other open problems, which are addressable with our existing code, or slightly modified versions thereof. We may study the effect of various open boundaries, for instance. It would also be possible to include additional terms in the Hamiltonian, which describe phonon interactions or external magnetic fields [49]. There are a number of possibilities which do not introduce a fermion sign problem.

Another problem of interest is to investigate the effect of interactions on the topological neck-disrupting Lifshitz transition that occurs in pure tight-binding models when the Fermi surface moves across a van Hove singularity in two dimensions, where the density of states diverges, and which can be interpreted as an excited state transition in the particle-hole excitation spectrum as shown in Ref. [50]. To study the role of interactions on this electronic transition, a chemical potential needs to be added. Unfortunately, this creates a fermion sign problem, which cannot be trivially removed. For the immediate future, however, we may add a spin-density chemical potential without sign problem similar to the staggered spin-density mass term used in this work and analogous to finite isospin chemical potential in QCD. One could then study the divergence in the corresponding susceptibility with finite-size scaling and see in what way the logarithmic divergence indicative of the neck-disrupting Lifshitz transition in two dimensions is modified by the interactions. Ultimately it would also be interesting to investigate whether the tight-binding model with interactions for the electronic excitations in graphene happens to belong to the class of theories in which a fermion sign problem can be dealt with in one way or another.

[1] A. K. Geim and K. S. Novoselov, Nat. Mater. **6**, 183 (2007).

[2] A. H. Castro Neto *et al.*, Rev. Mod. Phys. **81**, 109 (2009).

[3] V. N. Kotov *et al.*, Rev. Mod. Phys. **84**, 1067 (2012).

[4] C. W. J. Beenakker, Rev. Mod. Phys. **80**, 1337 (2008).

[5] K. S. Novoselov *et al.*, Nature (London) **438**, 197 (2005).

[6] Y. Zhang *et al.*, Nature (London) **438**, 201 (2005).

[7] G. W. Semenoff, Phys. Scripta T **146**, 014016 (2012).

[8] V. P. Gusynin *et al.*, Int. J. Mod. Phys. B **21**, 4611 (2007).

[9] K. S. Park, arXiv:1009.6033.

[10] E. M. C. Abreu, M. A. De Andrade, L. P. G. De Assis, J. A. Helayel-Neto, A. L. M. A. Nogueira, and R. C. Paschoal, J. High Energy Phys. 05 (2011) 001.

[11] A. Cortijo, M. A. H. Vozmediano, Nucl. Phys. B **763**, 293 (2007).

[12] A. Iorio and G. Lambiase, arXiv:1308.0265.

[13] J. E. Drut and T. A. Lähde, Phys. Rev. Lett. **102**, 026802 (2009).

[14] J. E. Drut and T. A. Lähde, Phys. Rev. B **79**, 165425 (2009).

[15] J. E. Drut and T. A. Lähde, Phys. Rev. B **79**, 241405 (2009).

[16] J. E. Drut, T. A. Lähde, and L. Suoranta, arXiv:1002.1273.

[17] J. E. Drut and T. A. Lähde, PoS **Lattice 2011**, 074 (2011).

[18] S. Hands and C. Strouthos, Phys. Rev. B **78**, 165423 (2008).

[19] W. Armour, S. Hands, and C. Strouthos, Phys. Rev. B **81**, 125105 (2010).

[20] W. Armour, S. Hands, and C. Strouthos, Phys. Rev. B **84**, 075123 (2011).

[21] P. V. Buividovich, E. V. Luschevskaya, O. V. Pavlovsky, M. I. Polikarpov, and M. V. Ulybyshev, Phys. Rev. B **86**, 045107 (2012).

[22] J. Giedt, A. Skinner, and S. Nayak, Phys. Rev. B **83**, 045420 (2011).

[23] R. Brower, C. Rebbi, and D. Schaich, PoS **Lattice 2011**, 056 (2011).

[24] R. Brower, C. Rebbi, and D. Schaich, arXiv:1101.5131.

[25] P. V. Buividovich and M. I. Polikarpov, Phys. Rev. B **86**, 245117 (2012).

[26] M. V. Ulybyshev, P. V. Buividovich, M. I. Katsnelson, and M. I. Polikarpov, Phys. Rev. Lett. **111**, 056801 (2013)].

[27] D. Smith and L. von Smekal, PoS **Lattice 2013**, 048 (2013).

[28] D. C. Elias *et al.*, Nat. Phys. **7**, 701 (2011).

[29] A. S. Mayorov *et al.*, Nano Lett. **12**, 4629 (2012).

[30] O. V. Gamayun, E. V. Gorbar, and V. P. Gusynin, Phys. Rev. B **81**, 075429 (2010).

[31] H. Leal, and D. V. Khveshchenko, Nucl. Phys. B **687**, 323 (2004).

[32] Y. Araki and T. Hatsuda, Phys. Rev. B **82**, 121403 (2010).

[33] Y. Araki, Ann. Phys. **326**, 1408 (2011).

[34] Y. Araki, Phys. Rev. B **85**, 125436 (2012).

[35] T. O. Wehling, E. Şaşıoğlu, C. Friedrich, A. I. Lichtenstein, M. I. Katsnelson, and S. Blügel, Phys. Rev. Lett. **106**, 236805 (2011).

[36] C. Popovici, C. S. Fischer, and L. von Smekal, PoS **Confinement X**, 269 (2012).

[37] C. Popovici, C. S. Fischer, and L. von Smekal, Phys. Rev. B **88**, 205429 (2013).

[38] S. Sorella and E. Tosatti, Europhys. Lett. **19**, 699 (1992).

[39] I. F. Herbut, Phys. Rev. Lett. **97**, 146401 (2006).

[40] C. Honerkamp, Phys. Rev. Lett. **100**, 146404 (2008).

[41] Z. Y. Meng, T. C. Lang, S. Wessel, F. F. Assaad, and A. Muramatsu, Nature (London) **464**, 847 (2010).

[42] M.-T. Tran and K.-S. Kim, Phys. Rev. B **83**, 125416 (2011).

[43] S. Raghu, X.-L. Qi, C. Honerkamp, and S.-C. Zhang, Phys. Rev. Lett. **100**, 156401 (2008).

[44] J. Negele and H. Orland, *Quantum Many-Particle Systems* (Addison-Wesley, Redwood City, CA, 1988).

[45] S. Duane, A. D. Kennedy, B. J. Pendleton, and D. Roweth, Phys. Lett. B **195**, 216 (1987).

[46] M. A. Clark and A. D. Kennedy, Phys. Rev. Lett. **98**, 051601 (2007).

[47] C. Gattringer and C. Lang, *Quantum Chromodynamics on the Lattice: An Introductory Presentation*, Lecture Notes in Physics 788, (Springer, Berlin, Heidelberg, 2010).

[48] J. C. Sexton and D. H. Weingarten, Nucl. Phys. B **380**, 665 (1992).

[49] E. V. Gorbar, V. P. Gusynin, V. A. Miransky, and I. A. Shovkovy, Phys. Rev. B **66**, 045108 (2002).

[50] B. Dietz, F. Iachello, M. Miski-Oglu, N. Pietralla, A. Richter, L. von Smekal, and J. Wambach, Phys. Rev. B **88**, 104101 (2013).